

Spatial Dependence of Heat Flux Transients and Wetting Behavior During Immersion Quenching of Inconel 600 Probe in Brine and Polymer Media

G. RAMESH and K. NARAYAN PRABHU

Cooling curve analysis of Inconel 600 probe during immersion quenching in brine and polymer quench media was carried out. Thermal histories at various axial and radial locations were recorded using a high-speed data acquisition system and were input to an inverse heat-conduction model for estimating the metal/quenchant heat flux transients. A high performance smart camera was used for online video imaging of the immersion quenching process. Solution to two-dimensional inverse heat-conduction problem clearly brings out the spatial dependence of boundary heat flux transients for a Inconel 600 probe with a simple cylindrical geometry. The estimated heat flux transients show large variation on axial as well as radial directions of quench probe surface for brine quenching. Polymer quenching showed less variation in metal/quenchant heat flux transients. Shorter durations of vapor film, higher rewetting temperatures, and faster movement of wetting front on quench probe surface were observed with brine quenching. Measurement of dynamic contact angle showed better spreading and good wettability for polymer medium as compared to brine quenchant. The solid-liquid interfacial tension between polymer medium and Inconel substrate was lower compared with that of solution. Rewetting and boiling processes were nonuniform and faster on quench probe surface during immersion quenching in brine solution. For the polymer quench medium, slow rewetting, uniform boiling and repeated wetting were observed.

DOI: 10.1007/s11663-014-0038-7

© The Minerals, Metals & Materials Society and ASM International 2014

I. INTRODUCTION

QUENCH hardening for the attainment of superior metallurgical and mechanical properties of steel components is a commonly used method in heat-treating industries. The process involves heating of steel to austenitizing temperature in a controlled atmosphere followed by rapid quenching in a suitable quench medium. Heat transfer and wetting are the two important phenomena that occur during quenching that controls the final metallurgical and mechanical properties of the components. The important parameters which control the metallurgical transformation/heat-transfer condition during quenching are grouped into three categories: (i) workpiece characteristics (composition, mass, geometry, surface roughness, and condition); (ii) quenchant characteristics (density, viscosity, specific heat, thermal conductivity, and boiling temperature); and (iii) quenching facility (bath temperature, agitation rate, and flow direction). Of all these factors listed, only a few can be changed in the heat-treatment shop. The selection of optimum quenchant and quenching conditions both from the technological and economical points

of view is an important consideration.^[1] When hot steel components are quenched into a vaporizable liquid medium, the cooling of components occurs by three stages known as vapor blanket, nucleate boiling, and convective cooling stages (Figure 1). Further, the transition from vapor blanket to nucleate boiling leads to the formation of wetting front which is defined as the loci between the vapor film and the occurrence of bubbles. The wetting front moves on the cooling surface with a significant velocity. Based on the movement of the wetting front, wetting behavior during quenching is classified as (i) Non-Newtonian wetting (a wetting process that occurs over a long period of time); and (ii) Newtonian wetting (a wetting process that occurs in a short time period or an explosion-like wetting process). A Newtonian type of wetting usually promotes uniform heat transfer and minimizes the distortion and residual stress development. In extreme cases of non-Newtonian wetting, because of large temperature differences, considerable variations in the microstructure and residual stresses are expected, resulting in distortion and the occurrence of soft spots.^[2] The quenching medium has a strong influence on the rewetting and heat-transfer behavior. Water, brine solutions, mineral oils, vegetable oils, and polymer media quenchants are generally used for quench hardening of steel components. Higher cooling rates are observed in all the three stages of quenching for water and brine solutions. For mineral oils, slow cooling rates in vapor- and convective-cooling stages and moderately fast cooling rates in

G. RAMESH, Senior Research Fellow, and K. NARAYAN PRABHU, Professor & Head, are with the Department of Metallurgical and Materials Engineering, National Institute of Technology Karnataka, Surathkal, Srinivasnagar, Mangalore 575 025, India. Contact e-mail: prabhukn_2002@yahoo.co.in, knprabhu.nitk@gmail.com

Manuscript submitted May 21, 2013.

Article published online February 22, 2014.

the nucleate boiling stage are observed. However, the cooling performance of the mineral oil is much lower than that of water.^[3] Further, the immersion of hot metal in water showed the start of wetting front at the lower edge of the sample followed by its ascend to the top in an almost annular manner. Similar to water, mineral oil shows similar rewetting behavior but with an additional wetting front at the upper edge of the metal.^[4] Polymer quenchants show intermediate cooling characteristics between water and oil and depict a wetting behavior different from quench media. Quenching of the component from high temperature is enough to raise the polymer to inverse solubility temperature in the vicinity of the metal/quenchant interface resulting in a polymer-enriched film formed around the hot metal. As the temperature of the hot surface decreases approximately to the Leidenfrost temperature, the vapor blanket explosively ruptures resulting in a pseudo-nucleate boiling process. The polymer film formation and subsequent rupture process may occur repetitively depending on the type of polymer.^[4,5] The cooling behavior of vegetable oil is different from that of the conventional or accelerated quench oil. Vegetable oils did not exhibit classical film boiling or nucleate boiling behavior during quenching, and the cooling is effected by convective heat transfer.^[6,7] Thus, assessment of heat transfer and wetting during quenching is an important topic for heat-treating engineers for producing a desired property distribution, acceptable microstructure, and minimize residual stresses in a particular section thickness of the component. Conductance measurement, three near-surface probe temperatures measurement, contact angle measurement, and online video recording of the quenching process are some of the techniques used to study the wetting behaviors of the quenchants.^[8,9] The heat-transfer characteristics of the quench media can be assessed by measurement of metal/quenchant heat-transfer coefficients and/or heat flux transients.

The surface heat flux or heat-transfer coefficient during quenching can be directly estimated by heat flux gage applied to a surface of the component or by determination of the temperature gradient at the component surface.^[10,11] However, the use of these methods requires special attention in designing sensors/probes. Most of the quenching heat-transfer research study involves the estimation of the surface heat-transfer coefficients/heat flux transients by measurement of the thermal history near the surface of quench probe during quenching. The measured temperature data and thermophysical properties of the metal are used to solve the heat-conduction equation inversely to determine the surface heat flux and temperature. Sequential function specification method,^[12,13] boundary element method,^[14] space marching finite difference method,^[15] Levenberg–Marquardt method,^[16] Laplace transform technique,^[17] advance–retreat method and golden section method,^[18] finite-difference method in conjunction with the least-square method,^[19] and iterative regularization algorithm^[20] are some of the techniques used in solving heat-conduction equation for estimating the surface heat flux transients/heat-transfer coefficients and

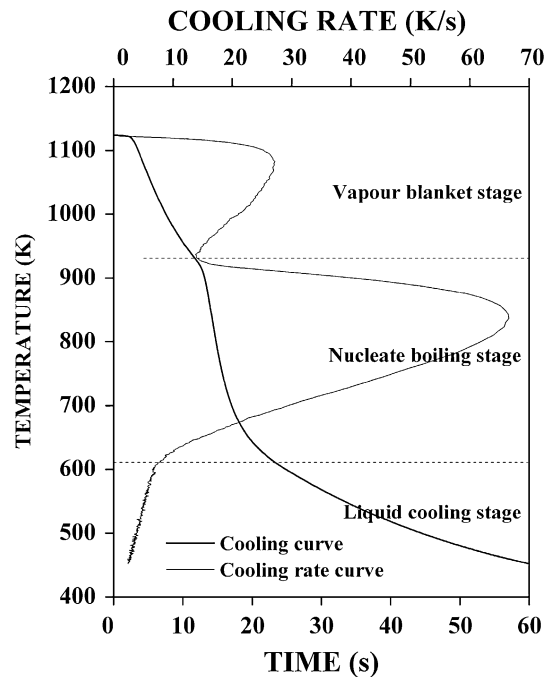


Fig. 1—Different stages of quenching.

temperature. However, most of the research studies on heat-transfer analyses during quenching involve estimation of only time-dependent single heat flux/heat-transfer coefficient.^[12–25] The formation of wetting front and its movement on hot metal surface during quenching result in simultaneous occurrence of all the three stages of quenching. Hence, the cooling conditions during quenching are time and location dependent. The literature on determination of spatially dependent heat flux/heat-transfer coefficient during immersion quenching is limited.^[26–30] The localized cooling of the component controls thermal transport and evolution of microstructure during quenching. Further, the simulation of quenching hardening process to predict the formation and/or distribution of microstructures and residual stresses requires the use of reliable boundary heat-transfer coefficients or heat flux transients at the surfaces of components. The assessment of spatially dependent heat-transfer coefficients/heat flux transients during quenching is therefore necessary to control the process parameters as well as for the effective utilization of the quench system.

In the present work, the thermal histories at axial and radial locations were measured during immersion quenching of cylindrical Inconel 600 probe in brine and polymer solutions. The temperature probe data and thermophysical properties were used as input to a finite-element-based inverse solver software to estimate the spatially dependent metal/quenchant heat flux transients and surface temperature. Wetting kinetics and kinematics of quench media were studied by measurement of dynamic contact angle, the online video imaging of the quench process, and estimation of spatially dependent surface temperatures of the probe.

II. EXPERIMENTAL PROCEDURE

Two quench probes of 12.5-mm diameter and 60-mm length were prepared from Inconel 600 material. To assess the axial variation of heat flux transients, holes of 1-mm diameter were drilled using Electric discharge machining (EDM) at different heights located at 2 mm from the surface (probe I) as shown in Figure 2(a). Holes designated as A7.5, A15, A22.5, A30, A37.5, A45, A52.5, and A40 and were located at 7.5, 15, 22.5, 30, 37.5, 45, 52.5, and 40 mm \pm 1 mm from the top surface of the quench probe, respectively. For determination of heat flux variations in the radial direction, holes of 1-mm diameter were drilled at different azimuth angles to a depth of 30 mm \pm 1 mm and were located at 2 mm from the surface (probe II) as shown in Figure 2(b). These holes, designated as R0, R45, R90, R135, R180, R225, R270, and R315 were located at azimuth angles of 0, 45, 90, 135, 180, 225, 270, and 315 deg, respectively. Holes of diameter 1 mm (AC for probe I and RC for probe II) were drilled at the geometric centers of both probes. New quench probes were conditioned by heating and quenching in quench oil for several times to obtain reproducible results. Further, the probes were continuously monitored by quenching in reference fluid (SERVOQUENCH 11, Indian Oil Corporation Ltd, India) between consecutive tests.

Brine solution (4 wt pct NaCl) and polymer solution (4 wt pct polyvinyl pyrrolidone K-30) were used as quenching media in the current study. Calibrated mineral-insulated K type Inconel 600 (Model: 219-4450, RS Components & Controls (India) Ltd, India) thermocouples of 1-mm diameter and 1-m length were used for measurement of thermal histories of the quench probes. The hot junction of thermocouples was tightly fitted into probe. Care was taken to ensure exact positioning of the hot junction of thermocouple in probe by marking the distance on thermocouple. Other ends of thermocouples were connected to a PC-based temperature data-acquisition system (NI 9213). Vertical tubular electric resistance furnace open at both ends was

used to preheat the quench probe to 1123 K (850 °C). The heating zone of the furnace was 80 mm in diameter, and had a length of 190 mm. During heating, the top and bottom parts of the furnace were covered with an insulating blanket. A quench tank of internal diameter of 115 mm and length of 210 mm with 2000 mL of quenchant was kept below the furnace during quenching. The quench probe support operated through guide pins was designed in such a way that the probe was positioned at the center of the heating zone during heating and at 50 mm from the the bottom surface of the quench tank during quenching. Once the probe attained the preheating temperature, it was directly quenched into the fluid without any significant time delay. The schematic of the experimental setup is shown in Figure 3. The probe temperatures were recorded at 0.1-second interval during quenching. A high-performance smart camera (NI 1774C) was used for online video monitoring of the quenching process. The scanning rate was three images per second. The probes were carefully cleaned by using acetone and washed thoroughly with water after each experiment.

The viscosities and thermal conductivities of brine and polymer solutions were measured using Ostwald viscometer and KD2 Pro thermal property analyzer respectively. Both viscosity and thermal conductivity were measured at an ambient temperature of 301 K (28 °C). FTA 200 (First Ten Angstroms) equipment was used to measure the liquid–vapor interfacial tension (γ_{lv}) and the spreading process of a liquid on a solid substrate. The equipment has a flexible video system for measuring the contact angle, and the surface and interfacial energies. Pendant drop method was used to measure the interfacial tension of quenchant. A 2.5-mL syringe with 0.9-mm-dia needle having a precision flow control valve was used for this purpose. For the study of spreading behavior, a droplet of quenchant was dispensed on to the Inconel 600 substrate, and the spreading phenomenon was recorded. The surface texture of the Inconel 600 substrate was similar to that

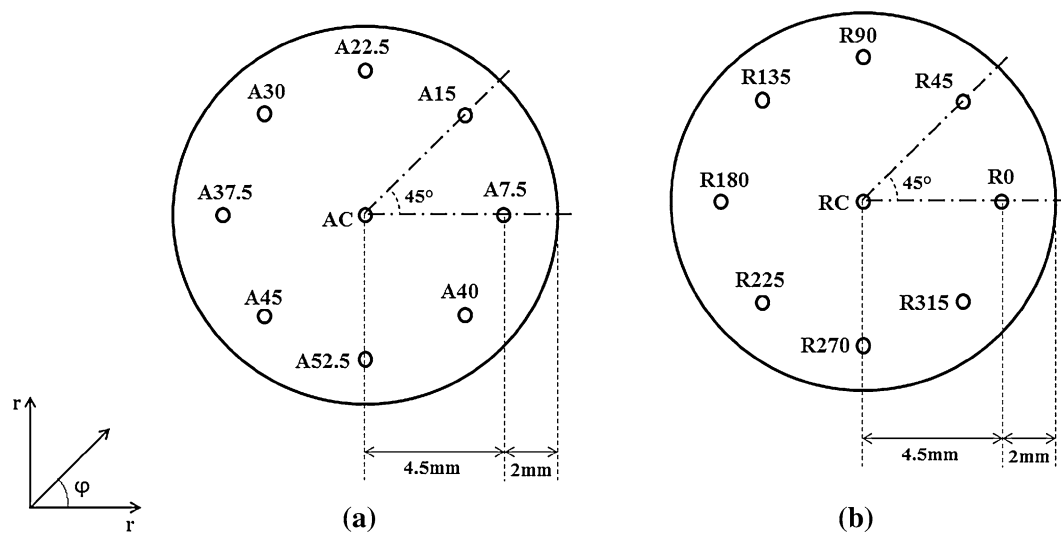


Fig. 2—Schematic of (a) probe I and (b) probe II.

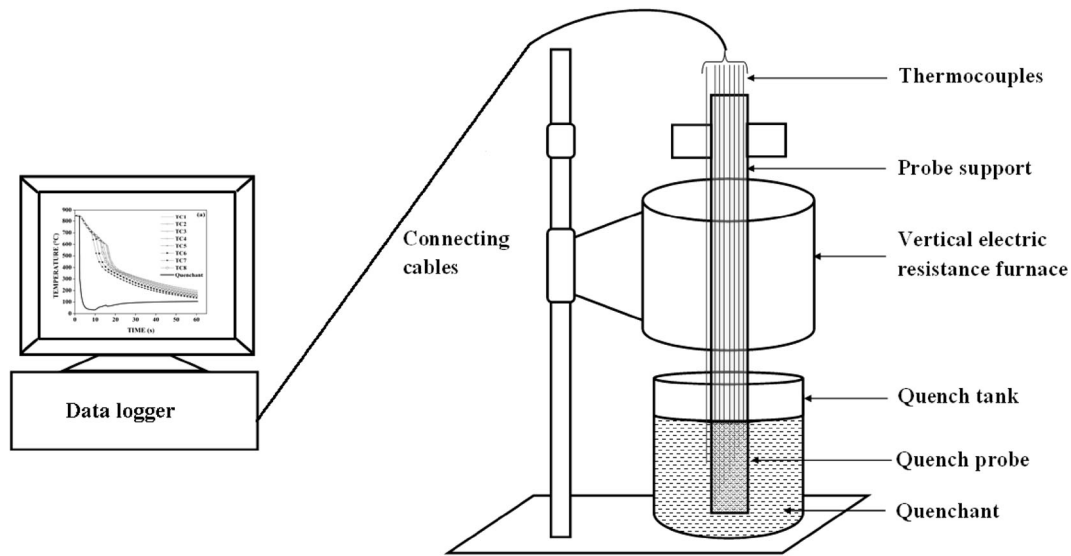


Fig. 3—Schematic of experimental setup.

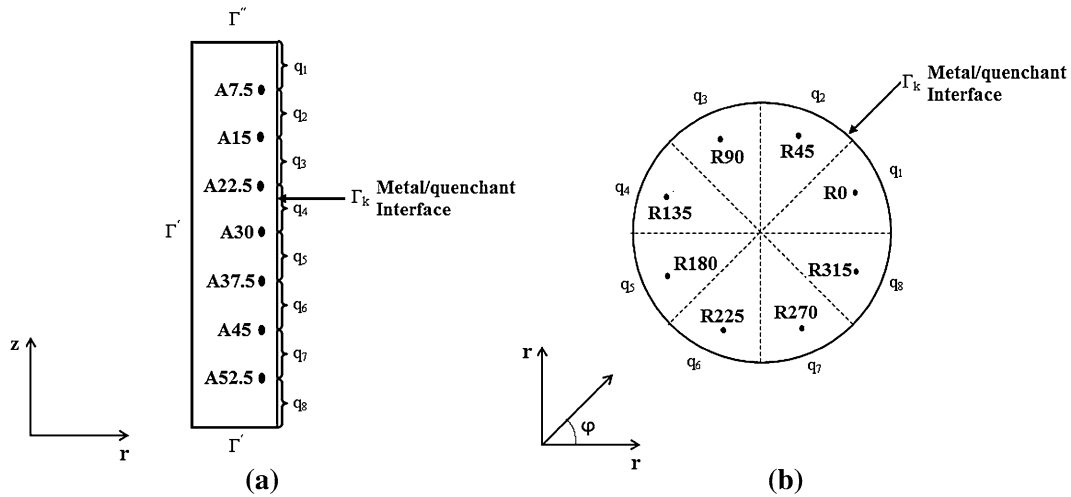


Fig. 4—Solution domains of (a) quench probe I and (b) quench probe II used in IHCP.

Table I. Thermophysical Properties of Inconel 600 Used in IHCP^[33]

Temperature (°C)	323	373	423	473	523	573	623	673	723	773	873	973	1073	1173
Thermal conductivity (W/mK)	13.4	14.2	15.1	16	16.9	17.8	18.7	19.7	20.7	21.7	—	25.9	—	30.1
Specific heat (J/kgK)	451	467	—	491	—	509	—	522	—	533	591	597	597	611
Density (kg/m ³)	8400	8370	—	8340	—	8300	—	8270	—	8230	8190	8150	8100	8060

of the Inconel 600 probe used for quenching experiments. Captured images were analyzed using FTA image analysis software to determine the interfacial tension and the contact angle. The experiments were carried out at an ambient temperature of 301 K (28 °C).

III. THEORETICAL BACKGROUND

The metal/quenchant interfacial heat flux transients were estimated from the measured temperature histories and the

thermophysical properties of the probe material using the inverse method. The equations that govern the two-dimensional transient heat conduction are given below:

$$\frac{1}{R} \frac{\partial}{\partial R} \left(\lambda R \frac{\partial T}{\partial R} \right) + \frac{\partial}{\partial z} \left(\lambda \frac{\partial T}{\partial z} \right) = \rho C_p \frac{\partial T}{\partial t} \quad [1]$$

$$\frac{1}{R} \frac{\partial}{\partial R} \left(\lambda R \frac{\partial T}{\partial R} \right) + \frac{1}{R^2} \frac{\partial}{\partial \phi} \left(\lambda \frac{\partial T}{\partial \phi} \right) = \rho C_p \frac{\partial T}{\partial t} \quad [2]$$

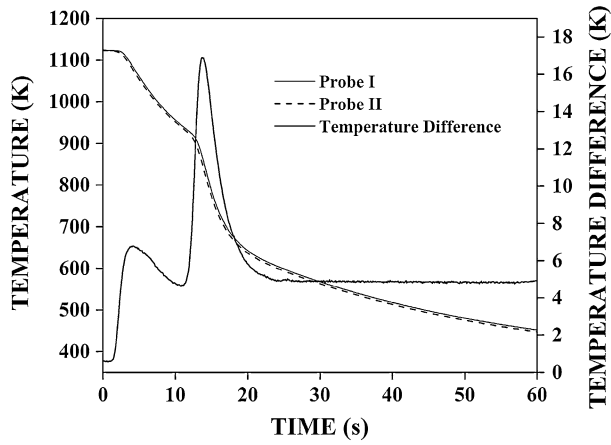


Fig. 5—Time–temperature data at geometric centers of two quench probes heated to 1123 K (850 °C) immersed in reference oil.

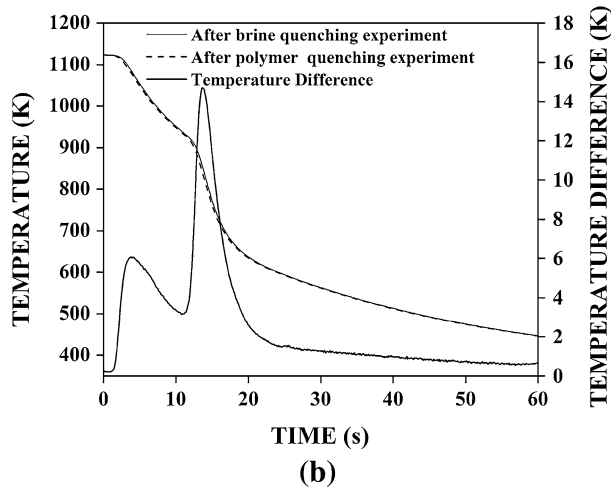
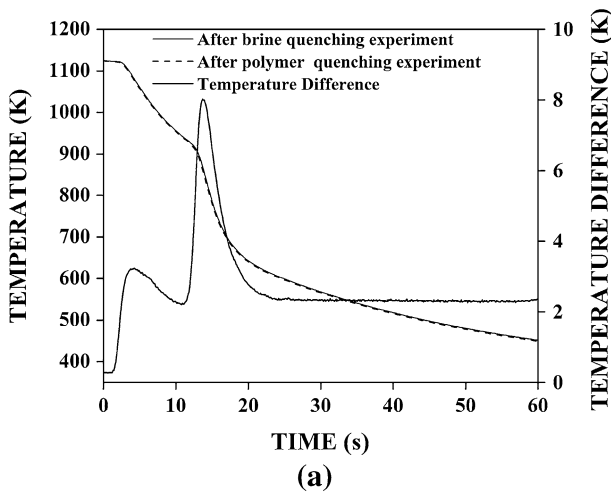


Fig. 6—Comparison of cooling curves of (a) probe I and (b) probe II against reference oil after quenching experiments with brine and polymer solutions.

for the axial and radial locations, respectively. The solution to IHCP was obtained using the finite-element-based inverse solver software, TmmFE (TherMet Solutions

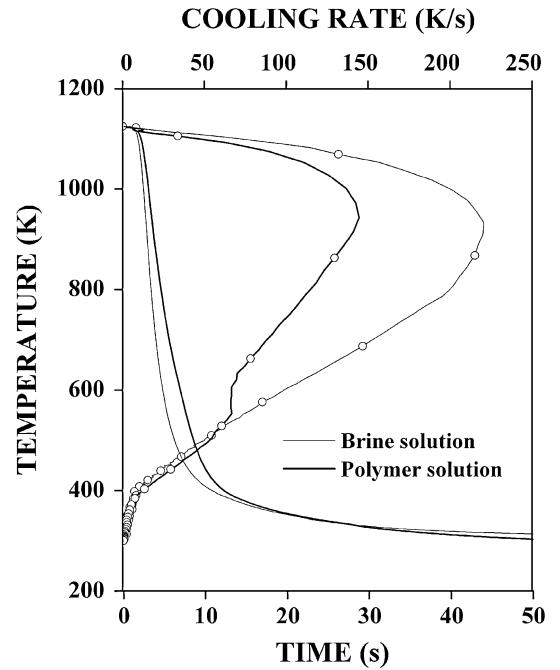


Fig. 7—Comparison of (a) cooling curves (line without symbol) and (b) cooling rate curves (line with symbol) of probe at the geometric center during quenching in brine and polymer solutions.

Pvt. Ltd., Bangalore, India). The Eqs. [1] and [2] were solved inversely with the following initial and boundary conditions for estimating the spatially dependent metal/quenchant heat transients.

The initial condition is

$$T(R, z) = T_i \quad \text{at } t = 0 \quad [3]$$

and the boundary conditions are

$$-\lambda \frac{\partial T}{\partial R} n_R - \lambda \frac{\partial T}{\partial z} n_z = q_k(R, z, t) \quad \text{on } \Gamma_k; \quad [4]$$

$$k = 1, 2, \dots, p, \dots, l$$

$$-\lambda \frac{\partial T}{\partial R} n_R - \lambda \frac{\partial T}{\partial z} n_z = 0 \quad \text{on } \Gamma' \quad [5]$$

$$-\lambda \frac{\partial T}{\partial R} n_R - \lambda \frac{\partial T}{\partial z} n_z = h(T - T_\infty) \quad \text{on } \Gamma'' \quad [6]$$

The detailed description of the mathematical solution and the implementation of the above serial inverse heat-conduction problem (IHCP) are given in References 31 and 32. This software adopts the following methodology for estimating heat flux transients. The unknown heat fluxes are first vectorized at the metal/quenchant interface surfaces as $(q_k)_i$; $k = 1, 2, \dots, p, \dots, l$ and $i = 1, 2, \dots, m, \dots, n$ (where k denotes the boundary segment, and i denotes the time step), and these heat fluxes are considered to be constant over the small interval of time Δt . The material properties (such as density, specific heat, and thermal conductivity as functions of temperatures), the initial condition, the boundary conditions, and the thermal histories at

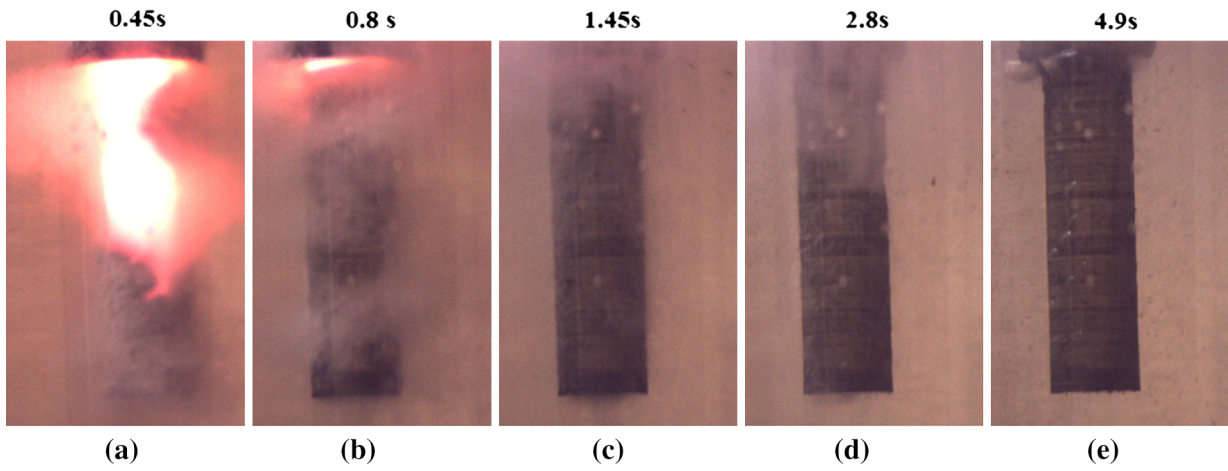


Fig. 8—Photographs of Inconel probe heated to 1123 K (850 °C) quenched in brine solution showing (a) formation of wetting front, (b) movement of wetting front to the top, (c and d) vapor mist formation and bubble boiling, and (e) liquid cooling on probe surface.

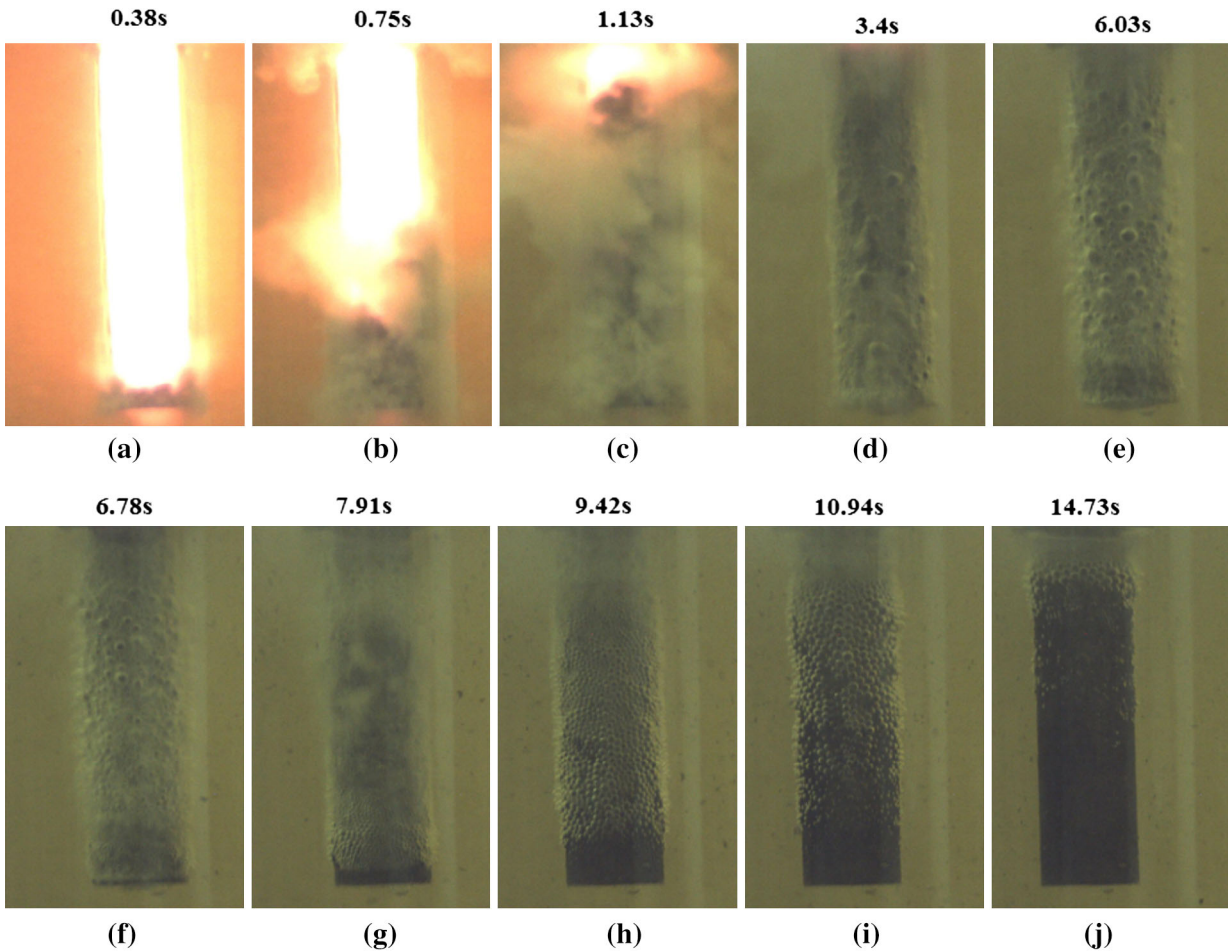


Fig. 9—Photographs of Inconel probe heated to 1123 K (850 °C) quenched in polymer solution showing (a) film formation and collapse of film by wetting front, (b) movement of wetting front, (c) strong vapor mist formation, (d-g) occurrences of bubble boiling, and (h-j) subsequent movement of nucleate boiling by liquid cooling on quench probe surface.

known locations are the required input parameters for the inverse program. Similar to the heat flux components, the thermal histories at the known locations are also vectorized into $Y_{j(i)}$; $j = 1, 2, \dots, s$ and $i = 1, 2, \dots, n$ (where j denotes the temperature sensor location). The

multiple heat flux components are calculated serially, one after the other, for every time step. The calculation procedure starts by assuming the flux vectors $(q_k)_i$, where $k = 1, 2, \dots, p, \dots, l$, $i = 1, 2, \dots, m - 1$; and $k = 1, 2, \dots, p - 1$; $i = 1, 2, \dots, m$ are the known entities,

Table II. Cooling Curve Parameters Determined for Brine and Polymer Quenchants

Critical Cooling Parameters	Brine Solution	Polymer Solution
CR_{peak} (K/s)	221	144
T_{CRpeak} (K)	911	943
CR_{705} (K/s)	210	141
CR_{550} (K/s)	205	120
CR_{300} (K/s)	84	66
CR_{200} (K/s)	37	43
$t_{730-260}$ (s)	3.22	4.86

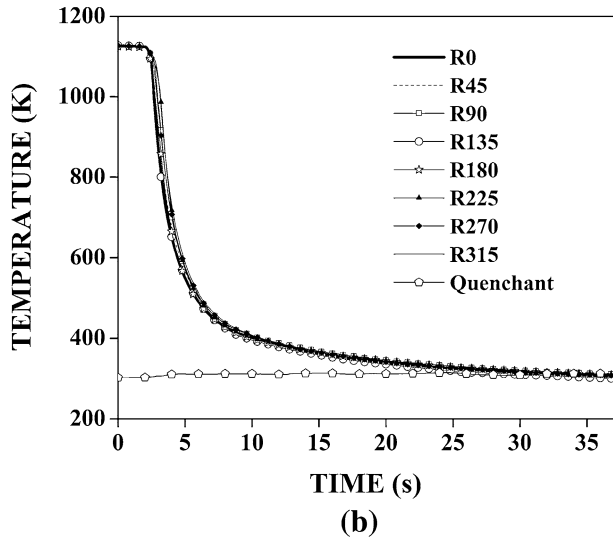
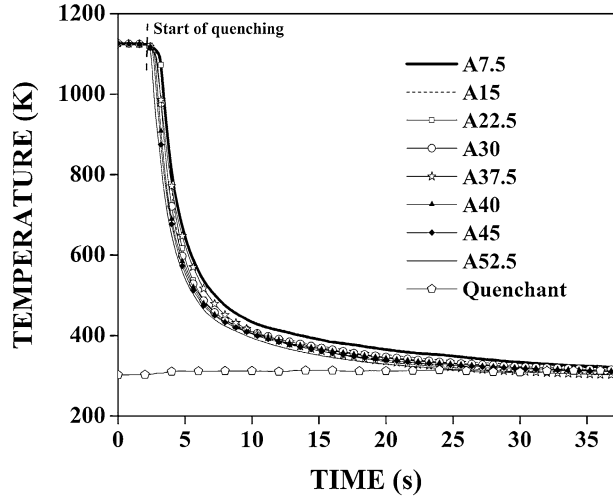


Fig. 10—Time-temperature data at (a) axial and (b) radial locations of Inconel probe heated to 1123 K (850 °C) immersed in brine solution.

and the aim is to find the heat flux $(q_p)_m$ (where p and m are the current segment and time step, respectively) for the time interval $t_{m-1} < t \leq t_m$. The sensitivity coefficients

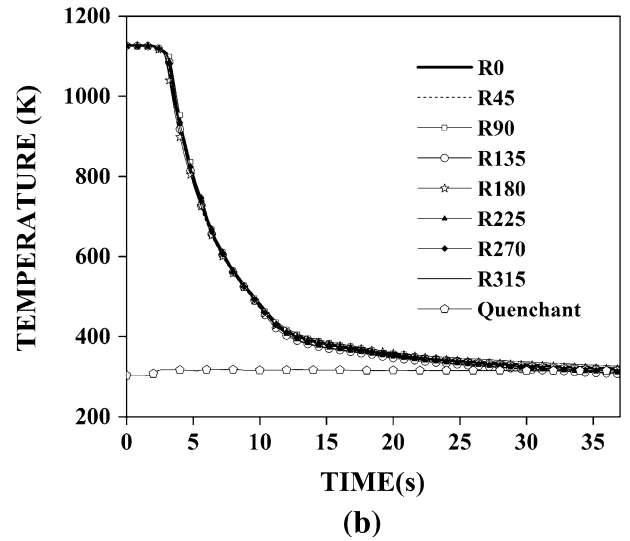
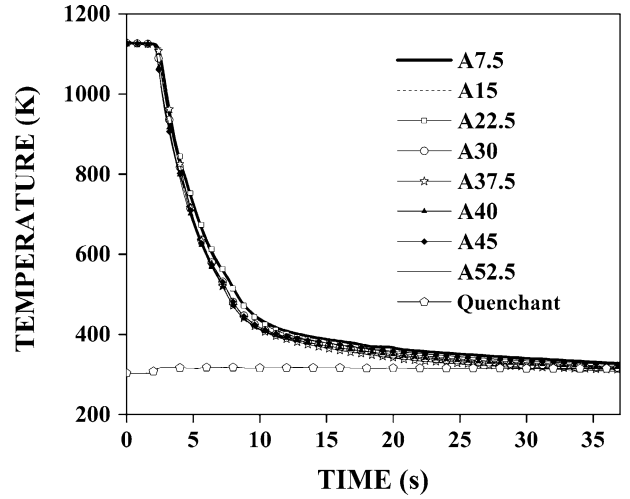


Fig. 11—Time-temperature data at (a) axial and (b) radial locations of Inconel probe heated to 1123 K (850 °C) immersed in polymer solution.

for all the sensor locations for r future time steps are now computed using the following equation:

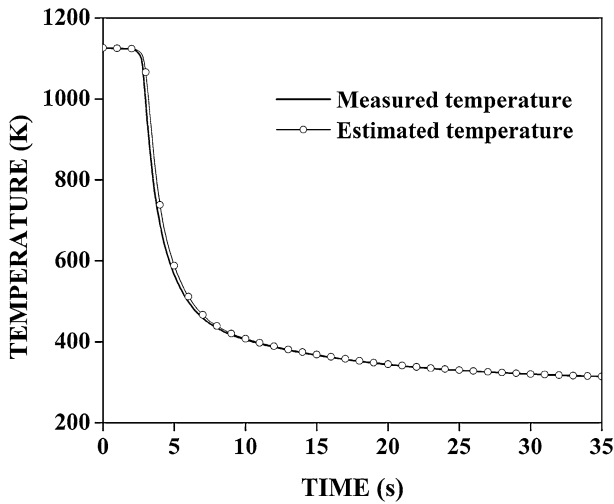
$$\phi_{j,k,i} = \frac{(\hat{T}_{j,k,i}^+ - \hat{T}_{j,k,i})}{q_{k,i}}; \quad i = m, \dots, m+r-1 \quad [7]$$

The numerator in the above equation is computed by solving the direct heat-conduction equation and is denoted as

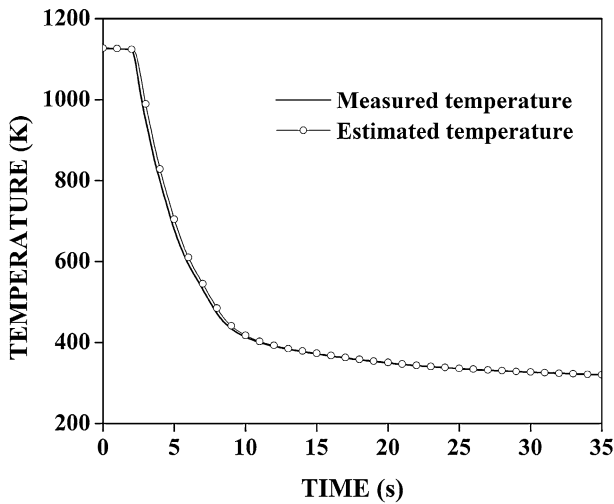
$$\hat{T}_{j,k,i}^+ = T_{j,k,i}(q_k)_{m,\dots,m+r-1} = (q_k)_{m-1}; \quad k = 1, \dots, p-1 \quad [8]$$

$$\hat{T}_{j,k,i} = T_{j,k,i}(q_k)_{m,\dots,m+r-1} = (q_k)_{m-1}; \quad k = 1, \dots, p-1 \quad [9]$$

The quantity $(q_p)^1$ is the updated heat flux in the current unknown boundary at the p th segment, which



(a)



(b)

Fig. 12—Measured and estimated temperature profiles of quench probe I at A40 location for quenching in (a) brine and (b) polymer media.

converges after a few iterations. The initial condition is taken as the thermal field resulting from the current distribution of the heat flux, and the direct solution is obtained by finite-element method for the time steps t_m to t_{m+r-1} . The heat flux at the p th boundary segment alone is then incremented by the value given by

$$(\nabla q_k)_m = \frac{\sum_{j=1}^J \sum_{i=1}^r [Y_{j,m+r-1} - \hat{T}_{j,k,m+r-1}] \phi_{j,k,i}}{\sum_{j=1}^J \sum_{i=1}^r (\phi_{j,k,i})^2} \quad [10]$$

The iteration is repeated until the absolute value of the ratio of the flux increment to the current value reaches a minimum. The remaining unknown heat flux components are computed in a similar manner.

Figure 4(a) shows the solution domain of half-symmetric shape of the quench probe I used for estimation of heat flux components in the axial direction. The

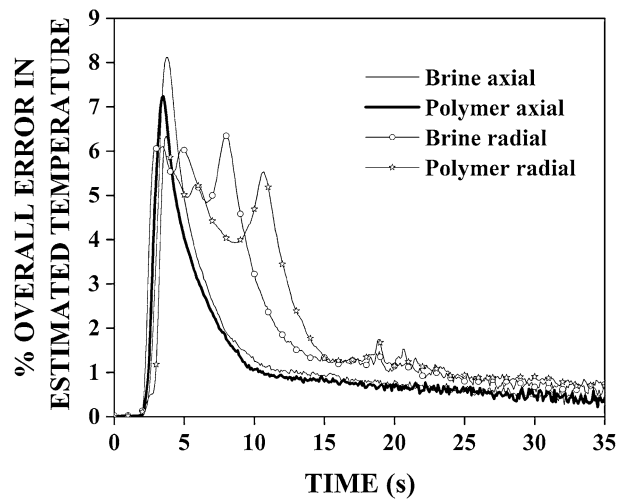


Fig. 13—Overall pct error in estimated temperatures of IHCP at axial and radial directions for brine and polymer quenchings.

geometry was discretized using four node quadrilateral and four side linear, uniform mesh. The total number of elements used in this case was 3000 (25×120). Similarly Figure 4(b) shows the solution domain of the quench probe II used for estimation of heat flux components in the radial direction. The geometry was discretized using three-node triangle and three-sided curved, uniform mesh. The total number of elements used in this case was 5000. Probe I and Probe II were divided into eight segments in the axial and radial directions respectively. An unknown heat flux boundary condition was assigned for each of these segments. The convergence limit for Gauss–Siedel iterations was set as 1×10^{-6} . The thermophysical properties of probe material used in the inverse model are given in Table I.^[33]

IV. RESULTS AND DISCUSSION

The thermal histories of two quench probes measured at geometric centers (AC and RC) during immersion quenching in reference fluid are shown in Figure 5. The plot shows that the cooling curves of two probes were comparable. The maximum temperature difference between the two probes was found to be 17 K (17 °C). Similarly, Figures 6(a) and (b) show cooling curves obtained at the geometric centers during quenching of probe I and probe II, respectively, in the reference fluid after carrying out quenching experiments with brine and polymer solutions. Maximum temperature differences were found to be 8 K and 15 K (−265 °C and −258 °C) for probe I and the probe II, respectively. The results confirm the repeatability of experiments with quench probes.

Figure 7 compares the cooling curves and cooling rates at the geometric centers of the probes obtained with brine and polymer quench media. The plot shows no clear characteristic feature of the vapor blanket stage. However, the video imaging of the quenching process showed the formation of the wetting front at the bottom of quench probe and its movement to the

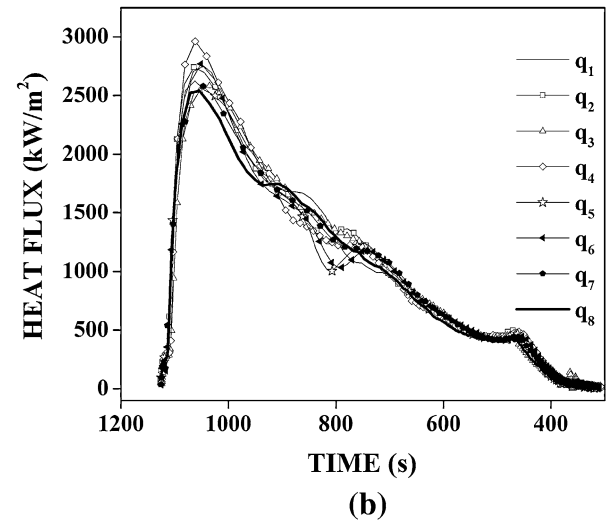
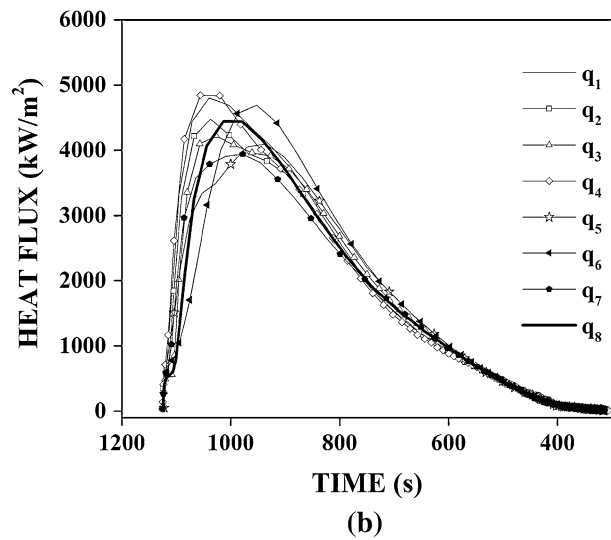
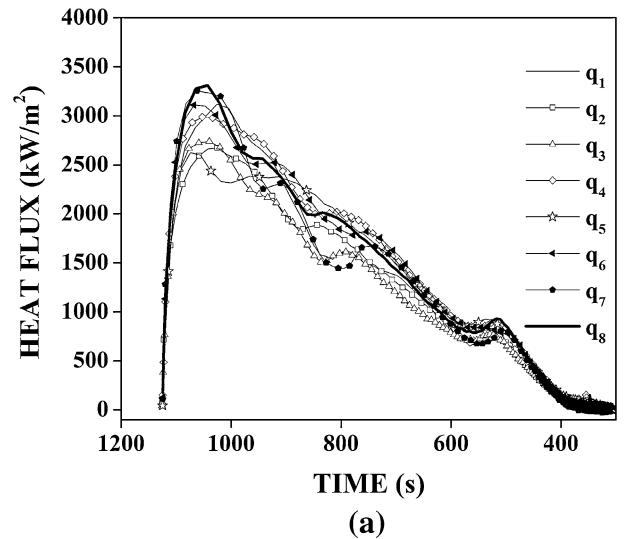
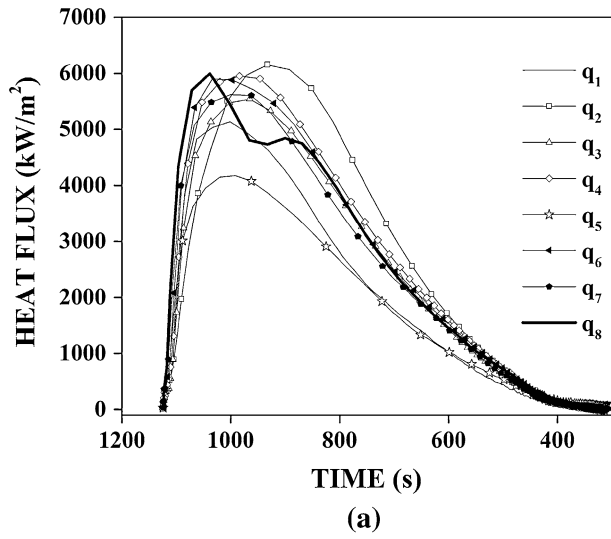


Fig. 14—Estimated metal/quenchant heat flux transients at (a) axial and (b) radial locations of probe surface during quenching in brine solution.

Fig. 15—Estimated metal/quenchant heat flux transients at (a) axial and (b) radial locations of probe surface during quenching in polymer solution.

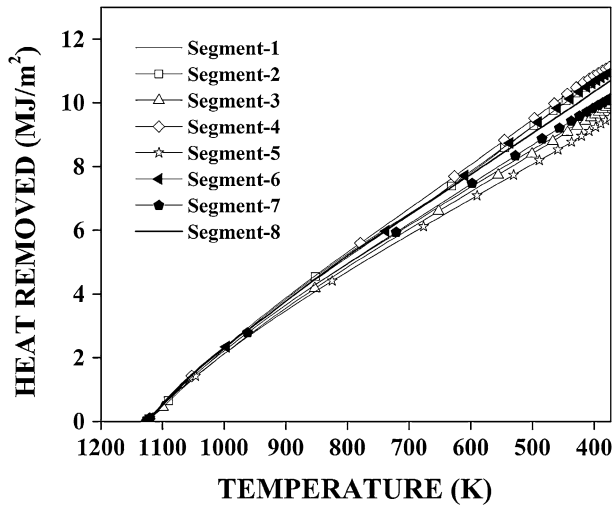
top (Figures 8 and 9). It indicates three stages of quenching, namely, vapor blanket, nucleate boiling, and convective cooling stages on quench probe surface during cooling in brine and polymer solutions. Moreover, both quenchant show rapid transition from vapor phase to nucleate boiling stage unlike that in mineral oil (Figure 4). From the plot, the critical cooling curve parameters, such as the peak cooling rate (CR_{peak}); the temperature of the peak cooling rate ($T_{CR_{peak}}$); the time to cool from 1003 K to 533 K (730 °C to 260 °C) ($t_{730-260}$); and the cooling rates at 978 K (705 °C) (temperature at which austenite transformation starts to occur for the most of the carbon steels), at 823 K (550 °C) (temperature which is at or near the nose of TTT curves for many steels), and at 573 K and 473 K (300 °C and 200 °C) (temperatures which are in the region of the martensitic transformation for many steels) designated as CR_{705} , CR_{550} , CR_{300} , and CR_{200} , respectively, were determined and are given in Table II. Brine

solution yielded higher values of cooling rates and lower value of $t_{730-260}$ indicating its higher cooling performance compared to polymer quenchant.

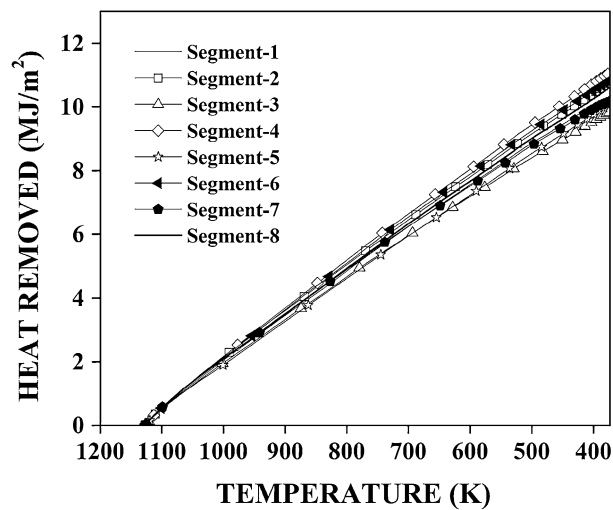
The thermal histories of quench probe measured at axial and radial locations during immersion cooling in brine (Figure 10) and polymer (Figure 11) solutions were used as inputs to the IHCP for estimating the spatially dependent heat flux transients and probe surface temperatures. The time-temperature data of quench probe I measured at different locations except A40 (40 mm from the top surface) were used as inputs to the inverse program, and the temperature measured at A40 location was used to compare the temperature estimated by the inverse program at the same location. In the case of probe II, all the thermal histories measured near to the surface were used as inputs to the inverse program. Figure 12 shows the comparison of the estimated and the measured temperatures at A40 location in probe I during quenching in brine and

polymer media. The overall error in the estimated temperatures for the whole domain was calculated using the equation^[31]:

$$\text{Pct Error in Estimated Temperatures} = \left| \frac{1}{n} \sum_{i=1}^n \left[\frac{T_{\text{measured}} - T_{\text{estimated}}}{T_{\text{measured}}} \times 100 \right]_i \right|, \quad [11]$$



(a)



(b)

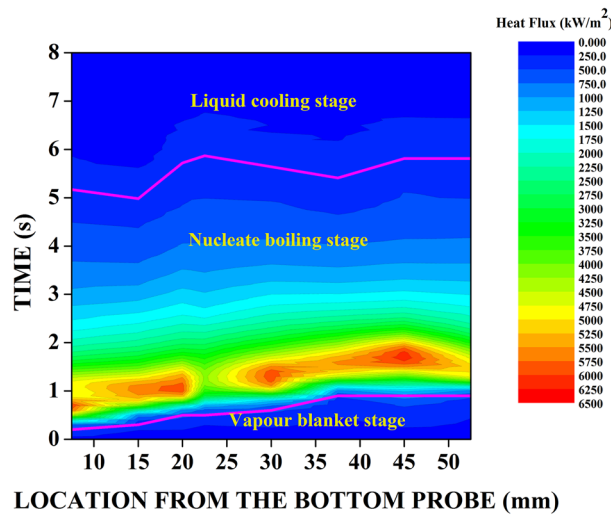
Fig. 16—Heat removed per unit area of probe during quenching in (a) brine and (b) polymer quenchants.

where “*n*” is the number of the unknown heat fluxes assigned at the quench probe surface. Figure 13 shows the overall pct errors in the estimated temperatures at axial and radial locations of probes for cooling in brine and polymer quenchants. The maximum overall pct errors of 8.12 and 7.24 were obtained for brine solution cooling in axial and radial directions, respectively. The corresponding values for polymer quenching were 6.35 and 6.35 pct, respectively.

The estimated metal/quenchant heat fluxes and surface temperatures for the probe surface segments in axial and radial locations are plotted for both quenchants and are shown in Figures 14 and 15, respectively. It was observed that heat flux increases from an initial to a peak value and then drops rapidly with decrease in probe temperature. The amount of heat removed during quenching was determined by plotting the integral heat flux curves for all quench media. Figure 16 shows the heat removed during quenching in brine and polymer solutions at different segments of probe with the temperature decreasing from 1123 K to 373 K (850 °C to 100 °C). The amounts of heat removed by quenchants were found to be 10.44 and 10.48 MJ/m² for brine and polymer quench media, respectively. The heat content of the probe was calculated using the formula $\frac{mC_p\Delta T}{A}$ (where *m*, *C_p*, *A*, and ΔT are the mass, specific heat capacity, area of the probe, and temperature difference, respectively), and was found to be 10.59 MJ/m². The heat removed by quenchants and the heat content of the quench probe were nearly the same indicating the validity of the inverse model used in the current study. The heat flux transients estimated at different surface locations in axial and radial directions show a similar trend. However, the magnitude of the heat flux is not the same for the considered segments in the axial as well as radial directions. This clearly indicates the spatial dependence of heat flux transients during immersion quenching. Table III shows the variation of the estimated peak heat flux values in axial and radial directions during quenching in brine and polymer solutions. For brine solution quenching, the maximum and the minimum peak heat flux values of 6153 and 4175 kW/m², respectively, were observed in axial location. Similarly, the maximum and the minimum peak heat flux values of 4844 and 3942 kW/m², respectively, were observed in radial location. The corresponding values for polymer quenching are 3310, 2625, 2960, and 2538 kW/m². Higher value of peak heat flux was observed for brine quenching compared with polymer quenching indicating higher quench severity of brine solution than that of

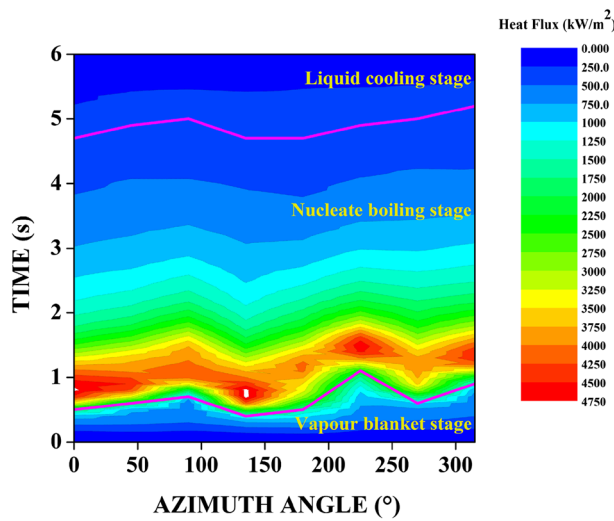
Table III. Estimated Metal/Quenchant Peak Heat Flux Values During Quenching in Brine and Polymer Media

Quench Medium	Probe	Peak Heat Flux (kW/m ²)							
		<i>q</i> ₁	<i>q</i> ₂	<i>q</i> ₃	<i>q</i> ₄	<i>q</i> ₅	<i>q</i> ₆	<i>q</i> ₇	<i>q</i> ₈
Brine solution	axial	5138	6153	5539	5951	4175	5903	5624	5997
	radial	4801	4478	4222	4844	4097	4688	3942	4445
Polymer solution	axial	3116	2673	2738	2989	2625	3110	3253	3310
	radial	2747	2740	2580	2960	2624	2768	2578	2538



— Transition from vapour to nucleate boiling
(or) nucleate boiling to liquid cooling

(a)

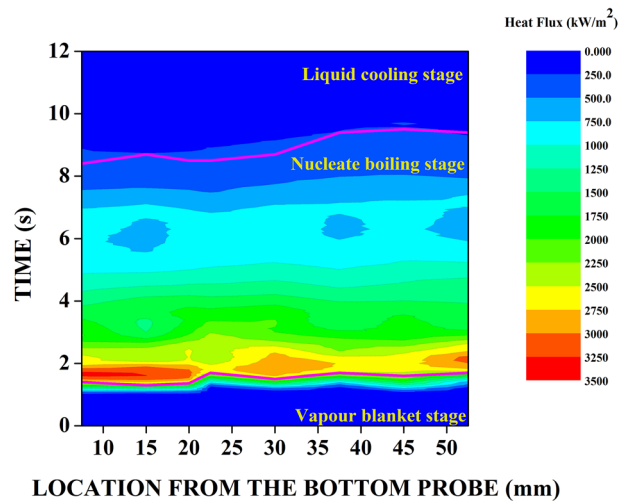


— Transition from vapour to nucleate boiling
(or) nucleate boiling to liquid cooling

(b)

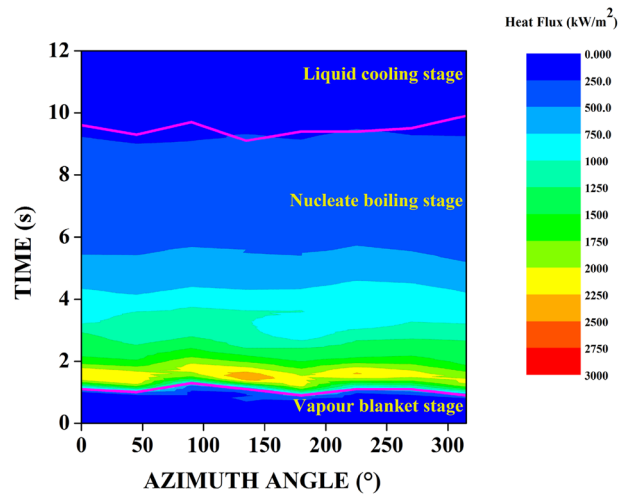
Fig. 17—Spatial distribution of heat fluxes in (a) axial and (b) radial directions of quench probe surface for brine quenching.

polymer medium. However, the variations in peak heat flux values of 1979 and 903 kW/m² for brine quenching and 684 and 422 kW/m² for polymer quenching were observed in axial and radial directions, respectively, indicating uniform cooling of the quench probe with polymer solution compared to that with brine solution. Figures 17 and 18 show spatial distributions of heat fluxes as a function of quench time in axial as well as radial locations for brine cooling and polymer cooling, respectively. From the estimated surface-temperature profiles of different segments in the axial locations, the duration of vapor blanket (from start of quenching to film boiling to nucleate boiling transition time), and the rewetting temperature (temperature of film boiling to



— Transition from vapour to nucleate boiling
(or) nucleate boiling to liquid cooling

(a)



— Transition from vapour to nucleate boiling
(or) nucleate boiling to liquid cooling

(b)

Fig. 18—Spatial distribution of heat fluxes in (a) axial and (b) radial directions of quench probe surface for polymer quenching.

nucleate boiling transition) were determined. Figure 19 shows the variation of rewetting temperature and wetting front velocity on quench probe surface. Brine quenching showed higher rewetting temperature and wetting front velocity compared to that with polymer quenching. The average rewetting temperatures of 1081 K and 1063 K (808 °C and 790 °C) were observed for quenching in brine and polymer solutions respectively. Average wetting front velocities of 47 and 27 mm/s were observed for brine and polymer solutions, respectively.

The metal/quenchant interfacial heat-transfer coefficient (h) was determined using the following relation:

$$h = \frac{q}{T_{\text{probe}} - T_{\text{quenchant}}}, \quad [12]$$

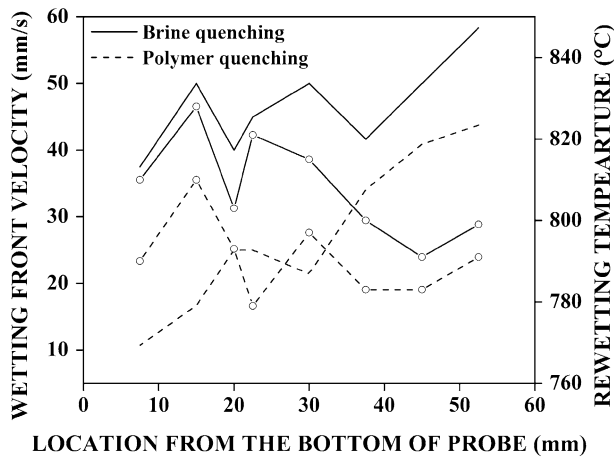


Fig. 19—Variation of wetting front velocity (line) and rewetting temperature (line with symbol) on axial locations of quench probe surface for brine and polymer quenchantings.

where q , T_{probe} , and $T_{\text{quenchant}}$ are the heat flux, the surface temperature of probe, and the fluid temperature, respectively. Figures 20 and 21 shows the surface heat-transfer coefficients during quenching in brine and polymer solutions. The heat-transfer coefficient curve showed occurrences of multiple peaks especially in the time range of 3 to 10 seconds for polymer quenching, while a continuous decrease from the initial peak was observed for brine quenching. This implies that the cooling behaviors of brine and polymer solutions are different. For better understanding of the cooling behaviors of fluids, quenching process was monitored by video imaging. The video images (Figures 8 and 9) taken during the quenchantings of Inconel probe in brine and polymer solutions show the formation of film and its collapse on quench probe surface. However, brine quenching showed rapid rewetting of fluid and non-uniform wetting on the quench probe surface. Further, the formation of mist on quench probe surface during rewetting was observed. This is due to the re-dissolution of salt layer formed at the early stage of quenching. In the case of polymer solution, a visible film and its collapse on quench probe surface were observed. The rewetting starts from the bottom of the quench probe surface and ascends to the top of quench probe. Similar to brine quenching, the formation of mist on the quench probe during film rupture was observed indicating re-dissolution of polymer into the solution. However, the mist formation on probe surface was uniform and of longer duration unlike that in brine solution. This clearly indicates the formation of thick film on quench probe surface in polymer quenching. During quenching in polymer medium, repeated rewetting of the fluid on quench probe surface was observed. In addition to this, numerous bubbles formed over the quench probe surface during nucleate boiling stage, and their subsequent movements led to the direct contact of the liquid medium with the probe surface.

The difference in the cooling behaviors of brine and polymer solutions is due to their respective chemical

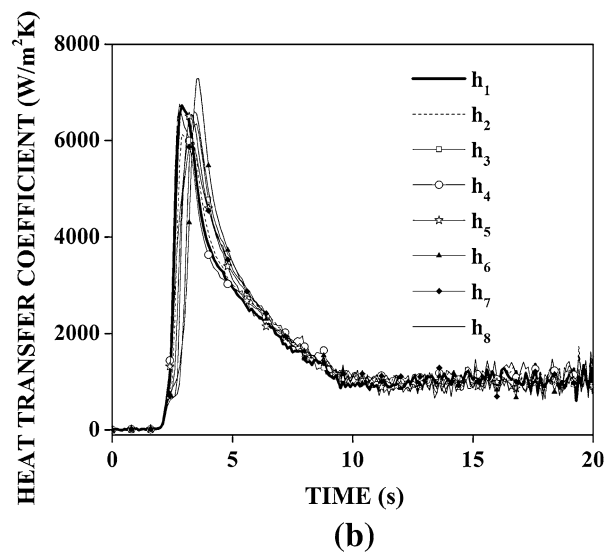
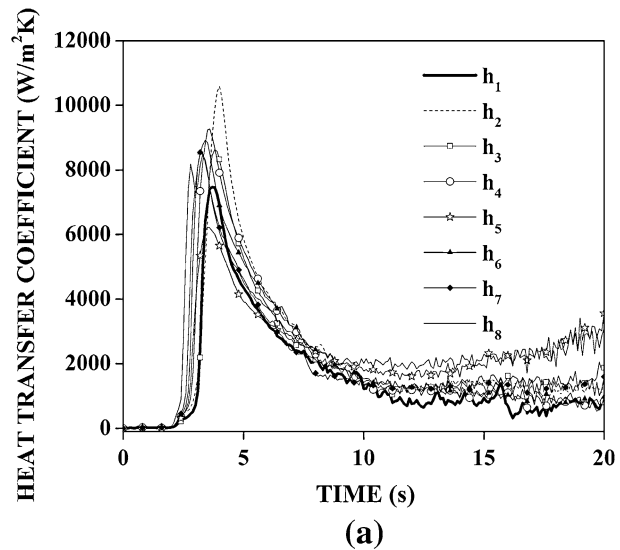
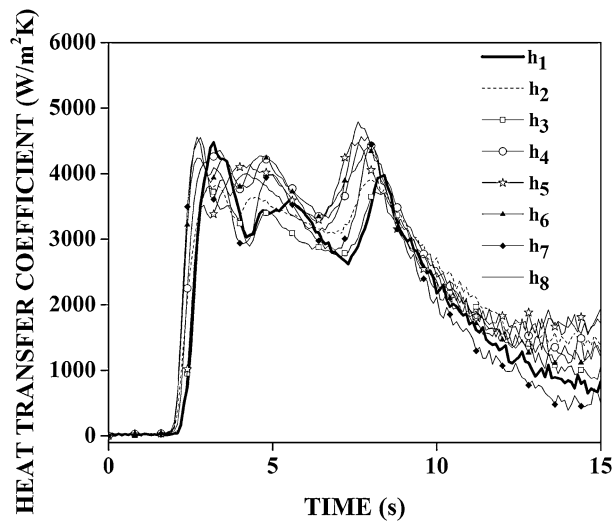
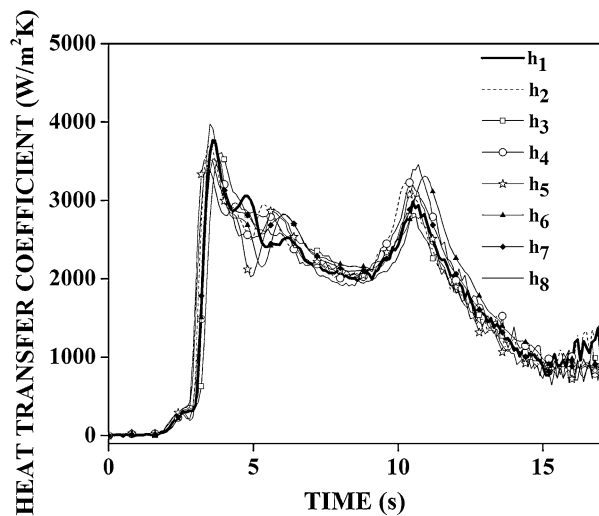


Fig. 20—Calculated surface heat flux transfer coefficients at (a) axial and (b) radial locations of probe surface during quenching in brine solution.

structures and thermophysical properties that have significant effects on the formation of vapor film, rewetting behavior, and nucleate boiling on the probe surface during quenching. When NaCl is added to water, the electrostatic attraction between the Na^+ and Cl^- is reduced, and they become separated. Since the water molecules are polar, the hydrogen atoms of each water molecule orient themselves toward the chloride ion, and oxygen atoms of each water molecule orient themselves toward the sodium ion. PVP is a nonionic homopolymer of vinylpyrrolidone ($\text{C}_6\text{H}_9\text{NO}$) which dissolves in water by solvation of polymer chains through hydrogen-bonding interactions.^[34] Table IV shows the thermophysical properties of brine and polymer solutions. The thermal conductivities of both quenchantings were found to be similar in magnitude. However, the polymer solution had a higher viscosity and lower surface tension compared to brine solution.



(a)



(b)

Fig. 21—Calculated surface heat flux transfer coefficients at (a) axial and (b) radial locations of probe surface during quenching in polymer solution.

Table IV. Thermophysical Properties of Quenchants

Properties	Brine Solution	Polymer Solution
Thermal conductivity (W/mK)	0.575	0.570
Density (kg/m ³)	1037	1034
Viscosity (cP)	1.05	1.829
Surface tension (mN/m)	74.3	67.5

The relaxation curves of the contact angles of droplets of brine and polymer solutions on an Inconel 600 substrate are shown in Figure 22. It is observed that the relaxation of the contact angle of brine solution was gradual, indicating poor spreading. On the other hand, the polymer solution showed rapid relaxation of the contact angle at the early stage, indicating better

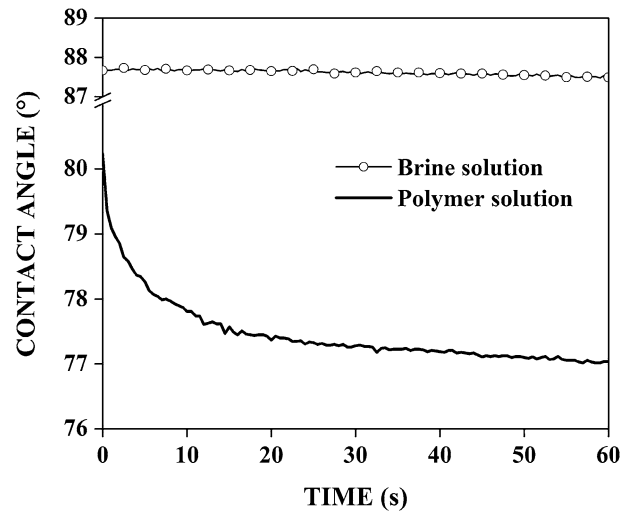


Fig. 22—Relaxation of contact angle of quenchant solutions on Inconel 600 substrate.

spreading. Further, a lower contact angle was observed for the polymer solution, indicating improved wettability compared to the brine solution. The basic mathematical relation for the wetting of a solid surface by a liquid is given by Young's equation^[35]

$$\cos \theta = \frac{\gamma_{sv} - \gamma_{sl}}{\gamma_{lv}}, \quad [13]$$

where “ γ ” represents the surface energy; the subscripts s, l, and v indicate solid, liquid, and vapor phases, respectively; and θ is the contact angle (θ) formed at the three-phase contact point. The above equation assumes that interfacial energies are under equilibrium condition, and the surface of solid is perfectly smooth. However, under the same solid-surface roughness and atmospheric conditions for different fluids, the quantity $\gamma_{lv} \cos \theta$ will give an idea about solid-liquid interfacial tension (γ_{sl}). The $\gamma_{lv} \cos \theta$ values of 3.11 and 14.96 mN/m were observed for brine and polymer solutions, respectively. It indicates that the solid-liquid interfacial tension between the polymer solution and Inconel 600 is lower compared with the brine solution-Inconel 600 interface. The contact angle (θ), when change in contact angle with time become less than 0.02 deg/s, was considered to be the equilibrium value. Lower the solid-liquid interfacial tension, the greater the spreading of fluid on substrate is, which resulted in the easier formation of vapor film on quench probe surface. Thus, quenching in polymer solution showed longer duration of vapor film stage, delayed rewetting, and lower rewetting temperature compared to that with brine quench medium. However, the polymer quenching shows uniform rewetting and boiling of fluid on quench probe surface. The spatial dependence of peak heat-transfer coefficients at 978 K, 823 K, 573 K, and 473 K (705 °C, 550 °C, 300 °C, and 200 °C) were determined and are shown in Figure 23. The variation in heat-transfer coefficients was more at axial locations than that at radial locations. Similarly, variation in the heat-transfer coefficient values was higher at peak, 978 K, and 823 K (705 °C and 550 °C) temperatures compared to that at 573 K and

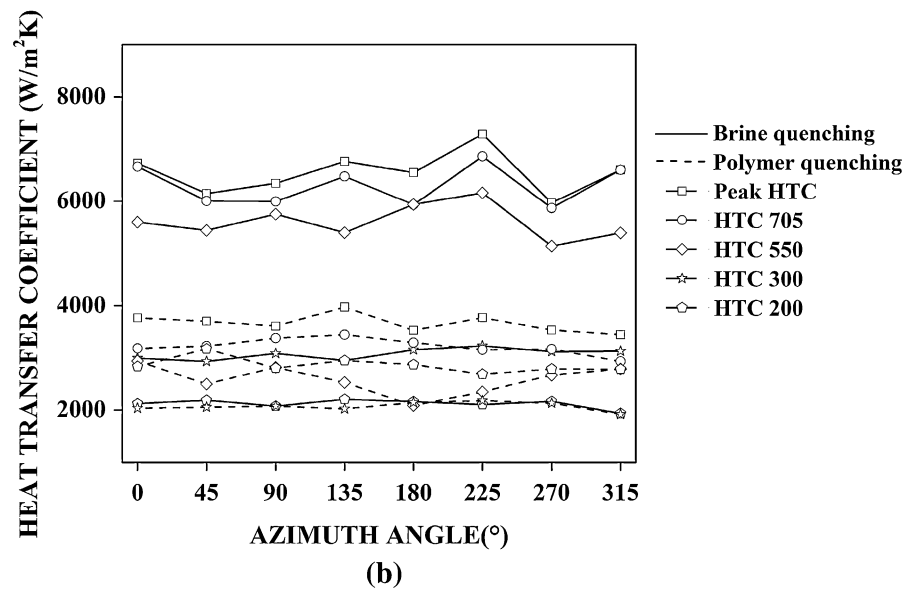
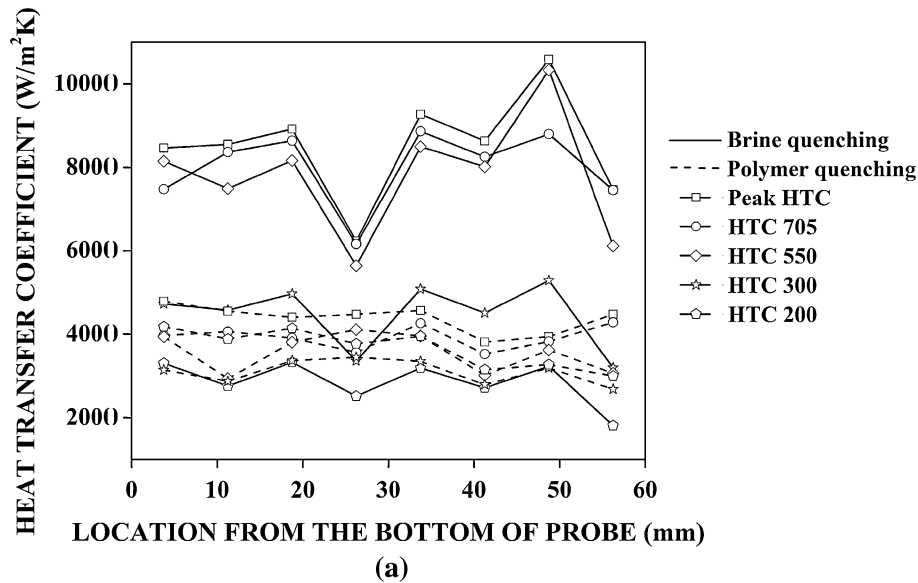


Fig. 23—Spatially dependent heat-transfer coefficients at critical temperatures in (a) axial and (b) radial locations on the probe surface during quenching.

473 K (300 °C and 200 °C). Polymer quenching showed lower heat-transfer coefficients with smaller variations on quench probe surface compared to that obtained with brine quenching. This is due to the the lower surface tension and solid–liquid interfacial tension of polymer solution, which improves the wettability of the fluid. Further, the higher viscosity of the polymer solution and the formation of the thick film during quenching result in lower heat-transfer coefficients compared to that obtained with brine medium.

V. CONCLUSIONS

The current investigation clearly brings out the spatial dependence of heat flux transients during quenching of a probe with a simple cylindrical geometry. The spatial variation in heat-transfer boundary condition was

confirmed by online video imaging during quenching. The following conclusions are drawn, based on the results and discussion of the current study.

1. Cooling curve analyses show three stages of cooling on the quench probe surface for both brine and polymer quenchants. The transition from vapor blanket to nucleate boiling stage was rapid in both quenchants.
2. Short vapor blanket stage, higher rewetting temperature, and fast movement of wetting front were observed for brine quenching.
3. Brine quenching shows maximum and minimum peak heat flux values of 6153 and 4175 kW/m², respectively, in axial location. In the radial direction, the corresponding values were 4844 and 3942 kW/m², respectively. The corresponding values for polymer quenching were 3310, 2625, 2960, and 2538 kW/m².

4. Variation in the estimated heat flux transients on axial as well as radial directions of quench probe was higher for brine quenching indicating nonuniform cooling of the probe in brine solution.
5. The relaxation of contact angle was gradual for brine solution, and rapid for polymer solution. Further, higher contact angle and solid-liquid interfacial tension were observed for brine solution on Inconel substrate compared with polymer solution. These indicate poor spreading and wettability of brine solution and better spreading, and improved wettability of polymer solution on Inconel substrate.
6. Online video imaging of the quenching process confirmed rapid and nonuniform rewetting and boiling of the fluid on the probe surface for brine quenching. On the other hand, polymer quenching was characterized by the formation of thick film, uniform rewetting, and boiling.

ACKNOWLEDGMENTS

One of the authors (KNP) thanks the Science and Engineering Research Board (SERB), Department of Science and Technology (DST), New Delhi, India for the research grant.

LIST OF SYMBOLS

z	Coordinate direction, m
R	Radius of probe, m
φ	Azimuth angles, deg
T	Temperature, K
C_p	Specific heat, J/kg K
t	Time, s
h	Heat-transfer coefficient, W/m ² K
q	Heat flux, W/m ²
k	Number of unknown heat flux components
j	Temperature sensor location, m
i	Time step, s
r	Future time step, s
\hat{T}	Temperature computed for a few future time steps, K
\hat{T}^+	\hat{T} with enhanced heat flux at the selected segment, K
Y	Measured temperature, K
n	Number of unknown heat flux segments assigned
λ	Thermal conductivity, W/mK
ρ	Density, kg/m ³
Γ	Domain surface boundary
ϕ	Sensitivity coefficient, Km ² /W
m	Mass, kg
A	Area, m ²
ΔT	Temperature difference, K
θ	Contact angle, deg
γ	Surface energy, mN/m

REFERENCES

1. B. Liscic: in *Quenching and Carburizing*, P.D. Hodgson, ed., The Institute of Materials, London, 1993, pp. 1–32.
2. C. Simsir and C.H. Gur: in *Handbook of Thermal Process Modeling Steels*, C.H. Gur and J. Pan, eds., CRC Press, Boca Raton, FL, 2008, pp. 341–475.
3. H.E. Boyer and P.R. Cary: *Quenching and Control of Distortion*, ASM International, Metals Park, OH, 1988, pp. 21–70.
4. H.M. Tensi, A. Stich, and G.E. Totten: *Proc. Int. Heat Treat. Conf. Equip. Process.*, Schaumburg, IL, 1994, pp. 243–51.
5. G.E. Totten: *9th International Induction Heat Treating Seminar*, Clearwater, FL, 2000. (http://www.quenchtek.com/pdf_files/technical_paper/Polymer%20Quenchants%20for%20Induction%20Heat%20Treating%20Applications%20The%20Basics.pdf). Accessed 8 Aug 2012.
6. G.E. Totten, H.M. Tensi, and K. Lainer: *J. Mater. Eng. Perform.*, 1999, vol. 8, pp. 409–16.
7. E.C. Souza, M.R. Fernandes, S.C.M. Augustinho, L.C.F. Canale, and G.E. Totten: *J. ASTM Int.*, 2009, vol. 6, Paper ID: JAI102188.
8. B. Liscic, H.M. Tensi, L.C.F. Canale, and G.E. Totten: *Quenching Theory and Technology*, 2nd ed., CRC Press, Boca Raton, FL, 2010, pp. 323–27.
9. K.N. Prabhu and P. Fernandes: *Metall. Mater. Trans. B*, 2007, vol. 38B, pp. 631–40.
10. T.E. Diller and S. Onishi: US Patent No. 4779994, 1988.
11. B. Liscic and T. Filetin: *J. Heat. Treat.*, 1988, vol. 5, pp. 115–24.
12. A.M. Osman and J.V. Beck: *J. Heat-transf.*, 1990, vol. 112, pp. 843–48.
13. B. Hernandez-Morales, J.K. Brimacombe, and E.B. Hawbolt: *J. Mater. Eng. Perform.*, 1992, vol. 1, pp. 763–71.
14. S. Das and A.J. Paul: *Metall. Trans. B*, 1993, vol. 24B, pp. 1077–86.
15. P. Archambault and A. Azim: *J. Mater. Eng. Perform.*, 1995, vol. 4, pp. 730–36.
16. P.-C. Chen, D.A. Kaminski and J.R.W. Messier: *Proc. 20th Conf.*, ASM International, St. Louis, MO, 2000, pp. 1125–31.
17. M. Monde: *Int. J. Heat Mass Transf.*, 2000, vol. 43, pp. 3965–75.
18. L. Huiping, Z. Guoqun, N. Shanting, and L. Yiguo: *Finite Elem. Anal. Des.*, 2006, vol. 42, pp. 1087–96.
19. H.-T. Chen and X.-Y. Wu: *Numer. Heat Transf. B*, 2006, vol. 50, pp. 375–94.
20. I. Felde: *J. Mech. Eng.*, 2010, vol. 56, pp. 77–83.
21. G. Stolz: *J. Heat Transf.*, 1960, vol. 82, pp. 20–25.
22. K.N. Prabhu and A.A. Ashish: *Mater. Manuf. Process.*, 2002, vol. 17, pp. 469–81.
23. H.-T. Chen and H.-C. Lee: *Int. J. Heat Mass Transf.*, 2007, vol. 50, pp. 2503–13.
24. C. Heming, L. Jianyun, L. Ziliang, H. Lijun, and H. Jie: *J. ASTM Int.*, 2008, vol. 5, Paper ID: JAI101813.
25. K. Babu and T.S.P. Kumar: *Int. J. Heat Mass Transf.*, 2011, vol. 54, pp. 106–17.
26. D.M. Trujillo and R.A. Wallis: *Ind. Heat.*, 1989, vol. 56, pp. 22–24.
27. S.G. Chen, C.-I. Weng, and J. Lin: *J. Mater. Process. Technol.*, 1999, vol. 86, pp. 257–63.
28. V. Sahai and S.M. Aceves: *Heat Transf. Eng.*, 2001, vol. 22, pp. 56–66.
29. H.K. Kim and S.I. Oh: *J. Mater. Process. Technol.*, 2001, vol. 112, pp. 157–65.
30. W.-L. Chen: *Int. J. Heat Mass Transf.*, 2012, vol. 55, pp. 597–606.
31. T.S. Kumar: *Numer. Heat Transf. B*, 2004, vol. 45, pp. 541–63.
32. S. Arunkumar, K.V. Sreenivas Rao, and T.S. Prasanna Kumar: *Int. J. Heat Mass Transf.*, 2008, vol. 51, pp. 2676–85.
33. R.N. Penha, L.C.F. Canale, G.E. Totten, G.S. Sarmiento, and J.M. Ventura: *J. ASTM Int.*, 2006, vol. 3, Paper ID: JAI13614.
34. G.E. Totten, C.E. Bates, and N.A. Clinton: *Handbook of Quenchants and Quenching Technology*, 1st ed., ASM International, Materials Park, OH, 1993, pp. 161–90.
35. C.J.V. Oss: *Interfacial Forces in Aqueous Media*, 2nd ed., CRC Press, Boca Raton, FL, 2006, pp. 25–50.